Physica E 130 (2021) 114662

Contents lists available at ScienceDirect

Physica E: Low-dimensional Systems and Nanostructures

journal homepage: http://www.elsevier.com/locate/physe

Control of Kerr nonlinearity in a four-level quantum system near a plasmonic nanostructure

Hamid Reza Hamedi [a,*], Vassilios Yannopapas [b], Algirdas Mekys [a], Emmanuel Paspalakis [c]

[a] Institute of Theoretical Physics and Astronomy, Vilnius University, Saulėtekio 3, Vilnius, LT-10257, Lithuania
[b] Department of Physics, National Technical University of Athens, Athens, 157 80, Greece
[c] Materials Science Department, School of Natural Sciences, University of Patras, Patras, 265 04, Greece

ARTICLE INFO

Keywords:
Non-linear optics
Plasmon
Nanostructure
Quantum system

ABSTRACT

We investigate the nonlinear optical response of a four-level double-V-type quantum system interacting with a pair of weak probe fields while located near a two-dimensional array of metal-coated dielectric nanospheres. Such a quantum system contains a V-type subsystem interacting with surface plasmons, and another V-type subsystem interacting with the free-space vacuum. A distinctive feature of the proposed setup is its sensitivity to the relative phase of the applied fields when placed near the plasmonic nanostructure. We demonstrate that due to the presence of the plasmonic nanostructure, the third-order (Kerr-type) susceptibility for one of the laser fields can be significantly modified while another probe field is acting. Moreover, the Kerr nonlinearity of the system can be controlled and even enhanced by varying the distance of the quantum system from the plasmonic nanostructure. We also show that the Kerr nonlinearity of such a system can be controlled by adjusting the relative phase of the applied fields. The results obtained may find potential applications in on-chip nanoscale photonic devices.

1. Introduction

Recently, it has been revealed that nonlinear optical effects can be significantly modified and eventually enhanced at the nanoscale when quantum systems are placed near plasmonic nanostructures. The strong modification of nonlinear effects is attributed to the large enhancement of the applied electric field, the substantial modification of the spontaneous decay rate, and the strong exciton-plasmon coupling for quantum systems near plasmonic nanostructures. Many interesting phenomena have been pointed out in this research area including gain without inversion [1–6], optical transparency and slow light [7–9], enhancement of the refractive index without absorption [8,10], electromagnetically induced grating [11,12], the manipulation of spontaneous emission [13–17], Fano effects in energy absorption [18–21], optical bistability [22–24], and enhanced second-harmonic generation [25,26], third-harmonic generation [27], and four-wave mixing [28–30].

Kerr nonlinearity, which is proportional to the third-order susceptibility, plays a crucial role in nonlinear and quantum optics. A large third-order nonlinear susceptibility [31–35] is of interest as it can be used for the realization of single-photon nonlinear devices [36,37]. However, for many years experimental research on quantum nonlinear optics has been limited due to the weak nonlinear response of the available materials. Recently, modification, and in particular enhancement, of the Kerr nonlinearity near plasmonic nanostructures have been proposed and analyzed [38–45].

A particular quantum system with interesting optical response is the four-level double-V quantum system. When located near a two-dimensional array of metal-coated dielectric nanosphere, this scheme exhibits quantum interference in spontaneous emission [15]. Namely, it was shown that optical transparency associated with slow light [7] and the strongly modified Kerr nonlinearity [39] appear in this system when interacting with a single weak probe beam of light near the periodic plasmonic nanostructure. If the system interacts with two laser fields, an extra degree of control can be realized exploiting the extra field as well as the phase difference of the applied fields. The later gives rise to phase dependent optical effects [5,8]. However, the control of Kerr nonlinearity for this quantum system under the interaction with two laser fields has not been yet analyzed.

In the present work, we explore the nonlinear optical properties of the four-level double-V-type quantum system interacting with a pair of weak probe fields and placed near a two-dimensional array of metal-coated dielectric nanospheres. The double-V-type system has two V-

* Corresponding author.
E-mail address: hamid.hamedi@tfai.vu.lt (H.R. Hamedi).

https://doi.org/10.1016/j.physe.2021.114662
Received 6 November 2020; Accepted 29 January 2021
Available online 15 February 2021

type subsystems. The upper V-type subsystem is influenced by its interaction with localized surface plasmons, while the other V-type subsystem interacts with the free-space vacuum. By means of a density matrix method, we calculate the linear and nonlinear optical susceptibilities for one of the laser fields in the presence of the other field and the plasmonic nanostructure. We demonstrate that the presence of the plasmonic nanostructure results in significant modification, and even enhancement, of the third-order nonlinear susceptibility for one of the probe fields. We find that the nonlinear optical susceptibility of the quantum system can be controlled through different external parameters such as the distance of the quantum system from the nanostructure as well as the relative phase between applied fields.

2. Theoretical model and formulation

The quantum system under study is presented in Fig. 1(a): a four-level system containing two closely lying upper states $|2\rangle$ and $|3\rangle$, and two lower states $|0\rangle$ and $|1\rangle$, making a four-level double-V quantum system. The quantum system is in vacuum and at distance d from the surface of the plasmonic nanostructure. It is placed right opposite the center of a nanosphere, i.e., at the center of the 2D unit cell of the (periodic) plasmonic nanostructure. At this (lateral) placement of the quantum system, the resulting quantum interference p is maximized. The states $|2\rangle$ and $|3\rangle$ denote two Zeeman sublevels ($J=1$, $M_J=\pm1$). The two lower states $|0\rangle$ and $|1\rangle$ are corresponding levels with $J=0$. One can define a dipole moment operator as

$$\vec{\mu}=\mu'(|2\rangle\langle 0|\hat{\epsilon}_-+|3\rangle\langle 0|\hat{\epsilon}_+)+\mu(|2\rangle\langle 1|\hat{\epsilon}_-+|3\rangle\langle 1|\hat{\epsilon}_+), \tag{1}$$

where $\hat{\epsilon}_\pm=(\mathbf{e}_z\pm i\mathbf{e}_x)/\sqrt{2}$ stand for the right-rotating ($\hat{\epsilon}_+$) and left-rotating ($\hat{\epsilon}_-$) unit vectors, while μ and μ' are real.

We assume that the quantum system interacts with two circularly polarized continuous-wave electromagnetic laser fields with total electric field

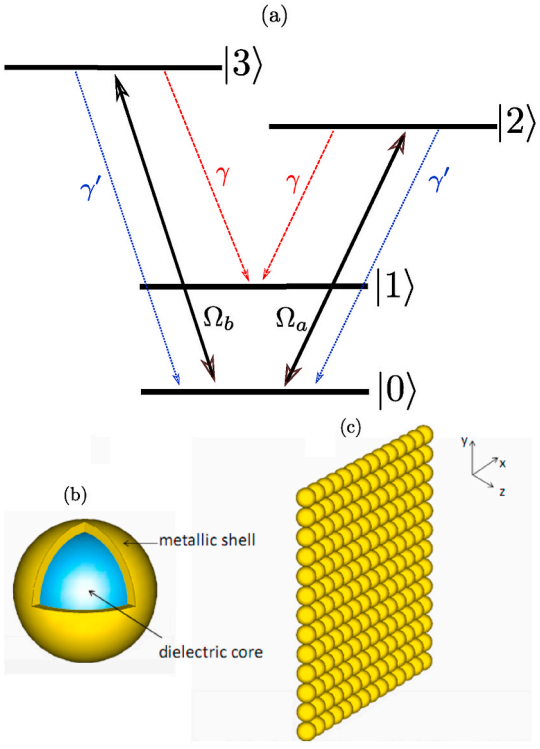

Fig. 1. Schematic diagram of the four-level double-V-type quantum system (a). A metal-coated dielectric nanosphere (b) and a 2D array of such spheres (c).

$$\vec{E}(t)=\hat{\epsilon}_+E_a\cos(\omega_a t+\varphi_a)+\hat{\epsilon}_-E_b\cos(\omega_b t+\varphi_b), \tag{2}$$

where $E_a(E_b)$ characterizes the electric-field amplitude, $\omega_a(\omega_b)$ denotes the angular frequency, and $\varphi_a(\varphi_b)$ is the individual phase for the field a (b). The laser field a acts between the lower level $|0\rangle$ and the upper state $|2\rangle$. The second laser field b couples the lower level $|0\rangle$ to the upper state $|3\rangle$. The transition $|0\rangle\leftrightarrow|1\rangle$ is dipole forbidden. Note that both fields are taken to have equal frequencies $\omega_a=\omega_b=\omega_L$.

Next, we assume that the upper V-type subsystem containing the states transitions $|2\rangle$, $|3\rangle$ and $|1\rangle$ lies within the surface-plasmon bands of the plasmonic nanostructure, whereas the lower V-type subsystem with states $|2\rangle$, $|3\rangle$ and $|0\rangle$ is spectrally distant from the surface-plasmon bands, and it is therefore not affected by the plasmonic nanostructure [15]. As a result, the spontaneous decay in lower V subsystem occurs because of the interaction of the quantum system with the free-space vacuum electromagnetic modes. This quantum system can be realized in hyperfine sublevels of D lines in alkali-metal atomic systems, such as ^{85}Rb and ^{87}Rb [8,9,17]. Similar interactions can also be realized in quantum dots, like in dual CdSe/ZnS/CdSe quantum dots [8,9]. The dynamics of the system is described from the master equation

$$\dot{\rho}_s=-\frac{i}{\hbar}[H_e,\rho_s]+\mathcal{L}\rho_s, \tag{3}$$

with

$$\begin{aligned}H_e &= \hbar\Big[\Big(-\delta-\frac{\omega_{32}}{2}\Big)|2\rangle\langle 2|+\Big(-\delta+\frac{\omega_{32}}{2}\Big)|3\rangle\langle 3|\\ &\quad-\Big(\frac{\Omega_a e^{i\varphi_a}}{2}|0\rangle\langle 2|+\frac{\Omega_b e^{i\varphi_b}}{2}|0\rangle\langle 3|+\text{H.c.}\Big)\Big],\end{aligned} \tag{4}$$

where $\Omega_a=\mu' E_a/\sqrt{2}\hbar$ and $\Omega_b=\mu' E_b/\sqrt{2}\hbar$ are the Rabi frequencies for the two fields. The parameter $\delta=\omega_L-\widetilde{\omega}$ is the detuning from resonance with the average transition energy of states $|2\rangle$ and $|3\rangle$ from state $|0\rangle$ [$\widetilde{\omega}=(\omega_2+\omega_3)/2-\omega_0$] and $\omega_{32}=(\omega_3-\omega_2)/2$, where $\hbar\omega_j=\hbar\omega_j$, $j=0$–3 is the energy of state $|j\rangle$. The operator $\mathcal{L}\rho_s$ in Eq. (3) represents the dissipation processes which is given by

$$\begin{aligned}\mathcal{L}\rho_s &= \gamma'(|0\rangle\langle 2|2\rho_s|2\rangle\langle 0|-|2\rangle\langle 2|\rho_s-\rho_s|2\rangle\langle 2|)\\ &\quad+\gamma'(|0\rangle\langle 3|2\rho_s|3\rangle\langle 0|-|3\rangle\langle 3|\rho_s-\rho_s|3\rangle\langle 3|)\\ &\quad+\gamma(|1\rangle\langle 2|2\rho_s|2\rangle\langle 1|-|2\rangle\langle 2|\rho_s-\rho_s|2\rangle\langle 2|)\\ &\quad+\gamma(|1\rangle\langle 3|2\rho_s|3\rangle\langle 1|-|3\rangle\langle 3|\rho_s-\rho_s|3\rangle\langle 3|)\\ &\quad+\kappa(|1\rangle\langle 3|2\rho_s|2\rangle\langle 1|-|2\rangle\langle 3|\rho_s-\rho_s|2\rangle\langle 3|)\\ &\quad+\kappa(|1\rangle\langle 2|2\rho_s|3\rangle\langle 1|-|3\rangle\langle 2|\rho_s-\rho_s|3\rangle\langle 2|)\\ &\quad+\gamma''(|0\rangle\langle 1|2\rho_s|1\rangle\langle 0|-|1\rangle\langle 1|\rho_s-\rho_s|1\rangle\langle 1|).\end{aligned} \tag{5}$$

The first two terms in Eq. (5) contain the free-space spontaneous decay $\gamma'=\Gamma_0$ [5]. The decay from the two upper states to the lower level is assumed to be the same. The energy difference of states $|2\rangle$ and $|3\rangle$ is rather small, i.e., ω_{32} is only a few Γ_0, where Γ_0 is the decay rate in free space [15]. The term involving γ'' is very small ($\gamma''\ll\gamma,\gamma'$) as it arises from a dipole forbidden transition. In this paper we neglect it by taking $\gamma''=0$.

The following equations are obtained for the density matrix elements by using Eq. (3) which describes the dynamics of the quantum system

$$\begin{aligned}\dot{\rho}_{20} &= \Big(i\delta+i\frac{\omega_{32}}{2}-\gamma-\gamma'\Big)\rho_{20}-\kappa\rho_{30}\\ &\quad+i\frac{\Omega_a}{2}(\rho_{00}-\rho_{22})-i\frac{\Omega_b}{2}e^{-i\varphi}\rho_{23},\end{aligned} \tag{6}$$

$$\begin{aligned}\dot{\rho}_{30} &= \Big(i\delta-i\frac{\omega_{32}}{2}-\gamma-\gamma'\Big)\rho_{30}-\kappa\rho_{20}\\ &\quad+i\frac{\Omega_b}{2}e^{-i\varphi}(\rho_{00}-\rho_{33})-i\frac{\Omega_a}{2}\rho_{32},\end{aligned} \tag{7}$$

$$\dot{\rho}_{23} = (i\omega_{32} - 2\gamma - 2\gamma')\rho_{23} + i\frac{\Omega_a}{2}\rho_{03} - i\frac{\Omega_b}{2}e^{i\varphi} - \kappa(\rho_{22} + \rho_{33}), \tag{8}$$

$$\dot{\rho}_{00} = 2\gamma'(\rho_{22} + \rho_{33}) - i\frac{\Omega_a}{2}(\rho_{02} - \rho_{20}) - i\frac{\Omega_b}{2}(\rho_{03}e^{-i\varphi} - \rho_{30}e^{i\varphi}), \tag{9}$$

$$\dot{\rho}_{22} = -2(\gamma + \gamma')\rho_{22} + i\frac{\Omega_a}{2}(\rho_{02} - \rho_{20}) - \kappa(\rho_{23} + \rho_{32}), \tag{10}$$

$$\dot{\rho}_{33} = -2(\gamma + \gamma')\rho_{33} + i\frac{\Omega_b}{2}(\rho_{03}e^{-i\varphi} - \rho_{20}e^{i\varphi}) - \kappa(\rho_{23} + \rho_{32}), \tag{11}$$

along with the population conservation $\rho_{00} + \rho_{11} + \rho_{22} + \rho_{33} = 1$ and $\rho_{ij} = \rho_{ji}^*$. The optical coherence corresponding to the probe transition of $|0\rangle \rightarrow |2\rangle$ ($|0\rangle \rightarrow |3\rangle$) is $\rho_{20}(\rho_{30})$, and the relative phase of the applied fields is denoted by $\varphi = \varphi_b - \varphi_a$. Note that the probe fields are assumed to be very weak so that one can treat them as a perturbation. In the above equations, the parameter κ is the coupling coefficient between states $|2\rangle$ and $|3\rangle$ due to spontaneous emission in a modified anisotropic vacuum [46] (anisotropic Purcell effect) which is responsible for the appearance of quantum interference [47].

The values of γ and κ are given by [13,14,48–52].

$$\gamma = \frac{\mu_0\mu^2\overline{\omega}^2}{2\hbar}\hat{e}_-.\,\mathrm{Im}\mathbf{G}(\mathbf{r},\mathbf{r};\overline{\omega}).\,\hat{e}_+, \tag{12}$$

$$\kappa = \frac{\mu_0\mu^2\overline{\omega}^2}{2\hbar}\hat{e}_+.\,\mathrm{Im}\mathbf{G}(\mathbf{r},\mathbf{r};\overline{\omega}).\,\hat{e}_+. \tag{13}$$

Here, $\mathbf{G}(\mathbf{r},\mathbf{r};\overline{\omega})$ [$\overline{\omega} = (\omega_3 + \omega_2)/2 - \omega_1$] describes the dyadic electromagnetic Green's tensor, while $\mathbf{r}$ and μ_0 refer to the position of the quantum emitter and the permeability of vacuum, respectively. One can obtain the values of γ and κ from Eqs. (12) and (13) as [13,14,48–52].

$$\gamma = \frac{\mu_0\mu^2\overline{\omega}^2}{2\hbar}\,\mathrm{Im}[G_\perp(\mathbf{r},\mathbf{r};\overline{\omega}) + G_\parallel(\mathbf{r},\mathbf{r};\overline{\omega})] = \frac{1}{2}(\Gamma_\perp + \Gamma_\parallel), \tag{14}$$

$$\kappa = \frac{\mu_0\mu^2\overline{\omega}^2}{2\hbar}\,\mathrm{Im}[G_\perp(\mathbf{r},\mathbf{r};\overline{\omega}) - G_\parallel(\mathbf{r},\mathbf{r};\overline{\omega})] = \frac{1}{2}(\Gamma_\perp - \Gamma_\parallel), \tag{15}$$

where $G_\perp(\mathbf{r},\mathbf{r};\overline{\omega}) = G_{zz}(\mathbf{r},\mathbf{r};\overline{\omega})$ and $G_\parallel(\mathbf{r},\mathbf{r};\overline{\omega}) = G_{xx}(\mathbf{r},\mathbf{r};\overline{\omega})$ show components of the electromagnetic Green's tensor, where the symbol $\perp(\parallel)$ refers to a dipole oriented normal, along the z axis (parallel, along the x axis) to the surface of the nanostructure. Let us also define the spontaneous emission rates normal and parallel to the surface as $\Gamma_{\perp,\parallel} = \mu_0\mu^2\overline{\omega}^2\,\mathrm{Im}[G_{\perp,\parallel}(\mathbf{r},\mathbf{r};\overline{\omega})]/\hbar$. The degree of quantum interference is then given by

$$p = (\Gamma_\perp - \Gamma_\parallel)/(\Gamma_\perp + \Gamma_\parallel). \tag{16}$$

When $p = \pm 1$ the maximum quantum interference is obtained in spontaneous emission [47]. This is achieved by placing the emitter close to a structure that completely quenches either $\Gamma_\perp$ or $\Gamma_\parallel$. When the emitter is placed in vacuum, $\Gamma_\perp = \Gamma_\parallel$ leading $\kappa = 0$, hence no quantum interference occurs in the system.

The plasmonic nanostructure considered here is a 2D array of touching metal-coated silica nanospheres [see Fig. 1(b) and (c)]. The dielectric function of the shell is provided by a Drude-type electric permittivity

$$\varepsilon(\omega) = 1 - \frac{\omega_p^2}{\omega(\omega + i/\tau)}, \tag{17}$$

where ω_p is the bulk plasma frequency and τ the relaxation time of the conduction-band electrons of the metal. A typical value of the plasma frequency for gold is $\hbar\omega_p = 8.99$ eV. This also determines the length scale of the system as $c/\omega_p \approx 22$ nm. The dielectric constant of SiO_2 is taken to be $\varepsilon = 2.1$. In the calculations we have taken $\tau^{-1} = 0.05\omega_p$. The lattice constant of the square lattice is $a = 2c/\omega_p$ and the sphere radius $S = c/\omega_p$ with core radius $S_c = 0.7c/\omega_p$. Using this particular choice of sphere/core radius and lattice constant we achieve maximization of the quantum interference rate p which prerequisite for the observation of the results present below.

For the calculation of the spontaneous decay rates next to the plasmonic nanostructure, we use the layered multiple scattering method [13,53–55]. We take $\overline{\omega} = 0.632\omega_p$ while the distance between the quantum system and the surface of the plasmonic nanostructure, d, varies from $0.5c/\omega_p$ to c/ω_p. For the results of $\Gamma_\perp$ and $\Gamma_\parallel$ that are used here, we refer to Fig. 3 in Ref. [7]. It is found that $\Gamma_\parallel$ gives significant suppression and its actual value is remarkably lower than the free-space decay rate. In addition, the value of $\Gamma_\perp$ decreases with increasing distance between the quantum system and the plasmonic nanostructure. For distances close to the plasmonic nanostructure, $\Gamma_\perp$ becomes much larger than the free-space decay rate. The value of $\Gamma_\perp$ is larger than the free-space decay rate for distances up to $0.6c/\omega_p$, while for distances between $0.65c/\omega_p$ and c/ω_p the value of $\Gamma_\perp$ becomes lower than the free-space decay rate.

3. Calculation of linear and nonlinear susceptibilities

In this section we calculate the linear and nonlinear electric susceptibilities for the laser field Ω_a. The probe fields are weak enough and are treated as perturbation to the system under steady-state condition. The method we use extends to third order the method presented in Ref. [56], and it is similar to that used in Ref. [57]. Under the weak-field approximation, the perturbation approach is applied to the density-matrix elements, which is expressed in terms of a perturbative expansion

$$\rho_{ij} = \rho_{ij}^{(0)} + \lambda\rho_{ij}^{(1)} + \lambda^2\rho_{ij}^{(2)} + \lambda^{(3)}\rho_{ij}^{(3)} + \ldots, \tag{18}$$

where λ is a continuously varying parameter ranging from zero to unity. The constituting terms $\rho_{ij}^{(n)}$ with $n = 1, 2, 3$ are of the nth order in the probe fields. Since the probe fields are assumed to be weak, the zeroth-order solution is $\rho_{00}^{(0)} = 1$, while the other elements $\rho_{ij}^{(0)} = 0$. Replacing Eq. (18) into Eqs. 6–11, the equations of motion for the first- and third order density-matrix elements are given by

$$\dot{\rho}_{20}^{(1)} = \left(i\delta + i\frac{\omega_{32}}{2} - \gamma - \gamma'\right)\rho_{20}^{(1)} - \kappa\rho_{30}^{(1)} + i\frac{\Omega_a}{2}, \tag{19}$$

$$\dot{\rho}_{30}^{(1)} = \left(i\delta - i\frac{\omega_{32}}{2} - \gamma - \gamma'\right)\rho_{30}^{(1)} - \kappa\rho_{20}^{(1)} + i\frac{\Omega_b}{2}e^{-i\varphi}, \tag{20}$$

and

$$\dot{\rho}_{20}^{(3)} = \left(i\delta + i\frac{\omega_{32}}{2} - \gamma - \gamma'\right)\rho_{20}^{(3)} - \kappa\rho_{30}^{(3)} + i\frac{\Omega_a}{2}(\rho_{00}^{(2)} - \rho_{22}^{(2)}) - i\frac{\Omega_b}{2}e^{-i\varphi}\rho_{23}^{(2)}, \tag{21}$$

$$\dot{\rho}_{30}^{(3)} = \left(i\delta - i\frac{\omega_{32}}{2} - \gamma - \gamma'\right)\rho_{30}^{(3)} - \kappa\rho_{20}^{(3)} + i\frac{\Omega_b}{2}e^{-i\varphi}(\rho_{00}^{(2)} - \rho_{33}^{(2)}) - i\frac{\Omega_a}{2}\rho_{32}^{(2)}. \tag{22}$$

After some lengthy but straightforward algebra we get

$$\rho_{20}^{(1)} = i\frac{\Omega_a}{2}S_1 - i\kappa\frac{\Omega_b}{2}e^{-i\varphi}S_2, \tag{23}$$

$$\rho_{30}^{(1)} = i\frac{\Omega_b}{2}e^{-i\varphi}S_3 - i\kappa\frac{\Omega_a}{2}S_2. \tag{24}$$

and

$$\rho_{20}^{(3)} = -a_2\kappa - a_1\left(i\delta - i\frac{\omega_{32}}{2} - \gamma - \gamma'\right) \tag{25}$$

$$\rho_{30}^{(3)} = -a_1\kappa - a_2\left(i\delta + i\frac{\omega_{32}}{2} - \gamma - \gamma'\right), \tag{26}$$

where

$$S_1 = \frac{\left(-i\delta + i\frac{\omega_{32}}{2} + \gamma + \gamma'\right)}{\left(-i\delta + i\frac{\omega_{32}}{2} + \gamma + \gamma'\right)\left(-i\delta - i\frac{\omega_{32}}{2} + \gamma + \gamma'\right) - \kappa^2}, \tag{27}$$

$$S_2 = \frac{1}{\left(-i\delta + i\frac{\omega_{32}}{2} + \gamma + \gamma'\right)\left(-i\delta - i\frac{\omega_{32}}{2} + \gamma + \gamma'\right) - \kappa^2}, \tag{28}$$

$$S_3 = \frac{\left(-i\delta - i\frac{\omega_{32}}{2} + \gamma + \gamma'\right)}{\left(-i\delta + i\frac{\omega_{32}}{2} + \gamma + \gamma'\right)\left(-i\delta - i\frac{\omega_{32}}{2} + \gamma + \gamma'\right) - \kappa^2}, \tag{29}$$

and

$$a_1 = \frac{-i\frac{\Omega_a}{2}(\rho_{00}^{(2)} - \rho_{22}^{(2)}) - i\frac{\Omega_b}{2}e^{-i\varphi}\rho_{23}^{(2)}}{\left(-i\delta + i\frac{\omega_{32}}{2} + \gamma + \gamma'\right)\left(-i\delta - i\frac{\omega_{32}}{2} + \gamma + \gamma'\right) - \kappa^2}, \tag{30}$$

$$a_2 = \frac{-i\frac{\Omega_b}{2}e^{-i\varphi}(\rho_{00}^{(2)} - \rho_{33}^{(2)}) - i\frac{\Omega_a}{2}\rho_{32}^{(2)}}{\left(-i\delta + i\frac{\omega_{32}}{2} + \gamma + \gamma'\right)\left(-i\delta - i\frac{\omega_{32}}{2} + \gamma + \gamma'\right) - \kappa^2}. \tag{31}$$

The second-order density matrix elements of Eqs. (25) and (26) featured in Eqs. (30) and (31) can be solved to obtain the steady-state solutions $\rho_{ij}^{(2)}$ (see Appendix A). In order to obtain the linear susceptibility $\chi^{(1)}$ and the third-order nonlinear susceptibility $\chi^{(3)}$, the susceptibility is assumed to be written as

$$\chi \approx \chi^{(1)} + 3\chi^{(3)}E_a^2/4. \tag{32}$$

Then, using

$$\chi(\delta) = \frac{\sqrt{2}N\mu'}{\epsilon_0 E_a}\rho_{20}, \tag{33}$$

and expanding ρ_{20} in perturbation series we get

$$\chi^{(1)}(\delta) = \frac{\sqrt{2}N\mu'}{\epsilon_0 E_a}\rho_{20}^{(1)} = \frac{N\mu'^2}{\epsilon_0\hbar}\frac{\rho_{20}^{(1)}}{\Omega_a}, \tag{34}$$

and

$$\chi^{(3)}(\delta)E_a^2 = \frac{4N\mu'^2}{3\epsilon_0\hbar}\frac{\rho_{20}^{(3)}}{\Omega_a}. \tag{35}$$

Substituting Eqs. 27–31 [and using Eqs. 44–50] into equations 23 and 25 and defining $x = \frac{\Omega_b}{\Omega_a}$, Eqs. (34) and (35) become

$$\chi^{(1)}(\delta) = \frac{N\mu'^2}{\epsilon_0\hbar}\frac{-i\kappa A + B\left(\delta - \frac{\omega_{32}}{2} + i\gamma + i\gamma'\right)}{\left(-i\delta + i\frac{\omega_{32}}{2} + \gamma + \gamma'\right)\left(-i\delta - i\frac{\omega_{32}}{2} + \gamma + \gamma'\right) - \kappa^2}, \tag{36}$$

and

$$\chi^{(3)}(\delta) = \frac{2N\mu'^4}{3\epsilon_0\hbar^3}\frac{-i\kappa C + D\left(\delta - \frac{\omega_{32}}{2} + i\gamma + i\gamma'\right)}{\left(-i\delta + i\frac{\omega_{32}}{2} + \gamma + \gamma'\right)\left(-i\delta - i\frac{\omega_{32}}{2} + \gamma + \gamma'\right) - \kappa^2}, \tag{37}$$

where here ϵ_0 is the vacuum permittivity and N is the density of the quantum systems, where A, B, C and D are defined in Appendix B.

The refraction part of the third-order susceptibility $\chi^{(3)}$ corresponds to the Kerr nonlinearity, while its imaginary part determines the nonlinear absorption. The real and imaginary parts of $\chi^{(1)}$ represent the linear dispersion and absorption, respectively. From Eqs. (36) and (37) one can clearly see that the expressions for the linear and nonlinear susceptibility are very similar in form with the only difference in their coefficients. So, one may expect to observe similar variation of the curves for $\chi^{(1)}$ and $\chi^{(3)}$ with the difference in their magnitude. However, this does not happen as the coefficients of the linear susceptibility does not depend on the detuning δ and the coefficients of the nonlinear susceptibility depends strongly on the detuning δ, so the frequency variation of the two susceptibilities is different. In addition, one can see that the linear and nonlinear susceptibilities $\chi^{(1)}$ and $\chi^{(3)}$ can be controlled by the system parameters such as the relative phase of applied fields φ.

4. Phase dependent Kerr nonlinearity

Next we study the nonlinear response of the quantum system to the probe field Ω_a for weak intensities via numerical simulation (the linear and nonlinear susceptibilities are plotted in units of $\frac{N\mu'^2}{\epsilon_0\hbar}$ and $\frac{2N\mu'^4}{3\epsilon_0\hbar^3}$, respectively). Fig. 2 shows the real and imaginary parts of $\chi^{(1)}$ and $\chi^{(3)}$ as a function of the detuning δ when the quantum system is in vacuum, i.e., without the plasmonic nanostructure. We assume that the two upper levels are degenerate ($E_2 = E_3$ leading to $\omega_{32} = 0$). This assumption significantly simplifies Eqs. (36) and (37) giving (for $\delta = 0$) analytical expressions for the linear as well as nonlinear absorption and dispersion coefficients (see Appendix C). The typical linear [Fig. 2(a)] and nonlinear [Fig. 2(b)] susceptibility spectra for this case are such that the medium experiences strong linear and nonlinear absorption at $\delta = 0$. This is already expected from Eqs. (36) and (37) when the quantum system is not near the plasmonic nanostructure ($\kappa = 0$ and $\gamma = \Gamma_0$). Setting $\kappa = 0$ and $\gamma = \Gamma_0$ into Eqs. (63)–(66), one can simplify these equations giving the resonant linear and nonlinear absorption and dispersion coefficients

$$\mathrm{Im}(\chi^{(1)}(\delta=0)) = \frac{N\mu'^2}{\epsilon_0\hbar}\frac{1}{(\Gamma_0 + \gamma')}, \tag{38}$$

$$\mathrm{Re}(\chi^{(1)}(\delta=0)) = 0, \tag{39}$$

$$\mathrm{Im}(\chi^{(3)}(\delta=0)) = \frac{2N\mu'^4}{3\epsilon_0\hbar^3}\frac{1-x^2}{8(\Gamma_0 + \gamma')^2}, \tag{40}$$

$$\mathrm{Re}(\chi^{(3)}(\delta=0)) = 0. \tag{41}$$

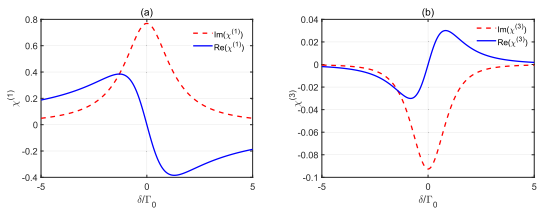

Fig. 2. (a) Linear susceptibility $\chi^{(1)}$ and (b) nonlinear susceptibility $\chi^{(3)}$ of the quantum system for the weak probe field Ω_a in arbitrary units as a function of the probe detuning δ in the absence of the plasmonic nanostructure. We have assumed that $\omega_{32} = 0$, $\gamma' = 0.3\Gamma_0$ and $\gamma'' = 0$.

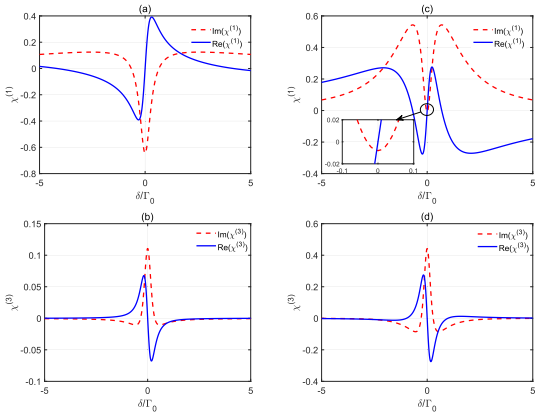

Fig. 3. (a,c) Linear susceptibility $\chi^{(1)}$ and (b,d) nonlinear susceptibility $\chi^{(3)}$ of the quantum system for the weak probe field Ω_a in arbitrary units as a function of the probe detuning δ in the presence of the plasmonic nanostructure. We take here $\omega_{32}=0$, $\gamma'=0.3\Gamma_0$, $\gamma''=0$, $x=1.5$, $\varphi=0$, $\overline{\omega}=0.632\omega_p$, and $d=0.3c/\omega_p$ (a,b), $d=0.6c/\omega_p$ (c,d).

On exact resonance, the Kerr nonlinearity is zero for the quantum system [see Fig. 2(b) and (Eq. (41))], while its magnitude is very weak around the resonance accompanied by the linear (Eq. (38)) and nonlinear (Eq. (40)) absorption. The slope of linear dispersion is negative around zero probe detuning suggesting superluminal light propagation [Fig. 2(a)]. We note that no phase dependence is obtained in this case.

The linear and nonlinear optical properties of the quantum system are very different when the quantum system is placed near the plasmonic nanostructure. In Fig. 3(a) and (c) where the quantum system is near the plasmonic nanostructure, we obtain a gain dip in the linear absorption profile at $\delta=0$. The slope of linear dispersion becomes positive, indicating slow light condition. As shown in Fig. 3(b) and (d), the enhanced Kerr nonlinearity appears inside the linear gain regions. The maximal Kerr nonlinearity around resonance is enhanced by almost four times when the distance between the quantum emitter and the nanostructure increases from $d=0.3c/\omega_p$ [Fig. 3(b)] to $d=0.6c/\omega_p$ [Fig. 3(d)].

As illustrated in Fig. 4, both $\chi^{(1)}$ and $\chi^{(3)}$are observed to behave differently for large distances of the quantum system from the plasmonic nanostructure. We observe that linear gain changes to a double-peaked absorption spectrum for $d=0.7c/\omega_c$ (Fig. 4(a)). The Kerr nonlinearity

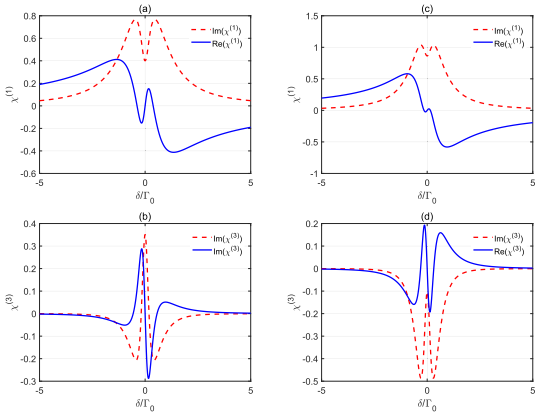

Fig. 4. (a,c) Linear susceptibility $\chi^{(1)}$ and (b,d) nonlinear susceptibility $\chi^{(3)}$ of the quantum system for the weak probe field Ω_a in arbitrary units as a function of the probe detuning δ in the presence of the plasmonic nanostructure. We take here $\omega_{32}=0$, $\gamma'=0.3\Gamma_0$, $\gamma''=0$, $x=1.5$, $\varphi=0$, $\overline{\omega}=0.632\omega_p$, and $d=0.7c/\omega_p$ (a,b), $d=0.8c/\omega_p$ (c,d).

find its maximal value around the zero probe field detuning [Fig. 4(b)]. In Fig. 4(d), nonlinear gain takes also place in the medium by altering the distance d (which leads to the change in values of $\Gamma_\perp$ and $\Gamma_\parallel$). We obtain different behaviors of $\chi^{(1)}$ and $\chi^{(3)}$. This is the main reason for appearance of gain or absorption in the quantum system as demonstrated in Figs. 3 and 4. The minima of linear (and nonlinear) absorption or gain in Figs. 3 and 4 are given by Eqs. (63) and (65)). One can show from Eq. (63), that the gain is present at $\delta=0$ when (Fig. 3)

$$\Omega_b > \frac{2\gamma'+\Gamma_\perp+\Gamma_\parallel}{(\Gamma_\perp-\Gamma_\parallel)\cos\varphi}\Omega_a, \tag{42}$$

while absorption takes place when (Fig. 4)

$$\Omega_b < \frac{2\gamma'+\Gamma_\perp+\Gamma_\parallel}{(\Gamma_\perp-\Gamma_\parallel)\cos\varphi}\Omega_a. \tag{43}$$

Eqs. (36) and (37) and their corresponding coefficients in Appendix B prove that in the presence of the plasmonic nanostructure, the linear and nonlinear susceptibilities are sensitive to the relative phase of the weak probe fields. Figs. 5 and 6 illustrate the dependence of $\chi^{(1)}$ and $\chi^{(3)}$ on φ when the quantum system is placed at a distance $d=0.4c/\omega_p$ from the surface of the plasmonic nanostructure. The strong variation of linear and nonlinear absorption and dispersion profiles for different values of φ is obvious. In particular, for $\varphi=0$ the maximal of Kerr nonlinearity is placed in a region of linear gain around $\delta=0$. Subluminal response takes place in this situation on resonance [see Figs. 5(a) and 6(a)]. When φ becomes π, a strong absorption instead of gain appears at line center for the $\chi^{(1)}$ profile, as can be seen in Fig. 5(c). Such a phase sensitive gain and absorption is well understood through Eqs. (42) and (43). In both cases, the value of the Kerr index at exact resonance is zero. According to Eq. (66), for $\varphi=0$ and $\varphi=\pi$, both sine terms in Eq. (66) vanish leading to zero Kerr nonlinearity on resonance. It should be mentioned that a nonzero resonant Kerr nonlinearity can be obtained for $\varphi=\pi/2$ [Fig. 6 (b)] and $\varphi=3\pi/2$ [Fig. 6(d)].

The results obtained here may suggest a tunable control over the Kerr nonlinearity of the quantum system near the plasmonic nanostructure by using the relative phase of the applied fields. In Fig. 7 we present an example of the variation of the Kerr nonlinearity spectra for different distances of the quantum system from the plasmonic nanostructure, $d=0.2c/\omega_p$ (dot line), $d=0.5c/\omega_p$ (dash line), $d=0.7c/\omega_p$ (solid line). A wide range of tunability can be observed over the refractive part of third-order nonlinear susceptibility $\chi^{(3)}$ spectra just by adjusting the

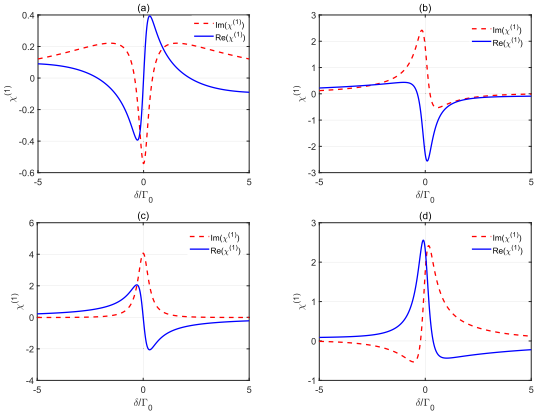

Fig. 5. Linear susceptibility $\chi^{(1)}$ of the quantum system for the weak probe field Ω_a in arbitrary units as a function of the probe detuning δ in the presence of the plasmonic nanostructure. We have assumed that $\omega_{32}=0$, $\gamma'=0.3\Gamma_0$, $\gamma''=0$, $x=1.5$, $\varphi=0$, $\overline{\omega}=0.632\omega_p$, $d=0.4c/\omega_p$ and (a), $\varphi=0$, (b), $\varphi=\pi/2$, (c) $\varphi=\pi$, and (d) $\varphi=3\pi/2$.

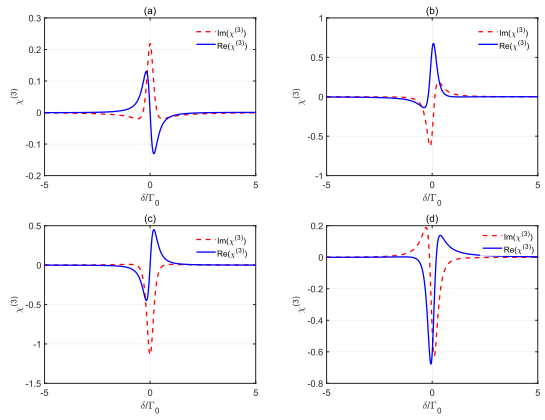

Fig. 6. Nonlinear susceptibility $\chi^{(3)}$ of the quantum system for the weak probe field Ω_a in arbitrary units as a function of the probe detuning δ in the presence of the plasmonic nanostructure. We have assumed that $\omega_{32} = 0$, $\gamma' = 0.3\Gamma_0$, $\gamma'' = 0$, $x = 1.5$, $\varphi = 0$, $\overline{\omega} = 0.632\omega_p$, $d = 0.4c/\omega_p$ and (a), $\varphi = 0$, (b), $\varphi = \pi/2$, (c) $\varphi = \pi$, and (d) $\varphi = 3\pi/2$.

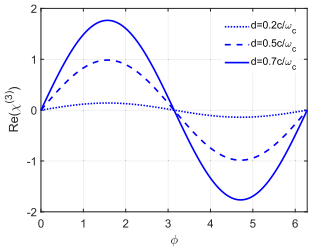

Fig. 7. The refractive part of third-order nonlinear susceptibility Re($\chi^{(3)}$) (Kerr nonlinearity) of the quantum system for the weak probe field Ω_a in arbitrary units as a function of the relative phase φ for different distances from the plasmonic nanostructure $d = 0.2c/\omega_p$ (dot line), $d = 0.5c/\omega_p$ (dash line), $d = 0.7c/\omega_p$ (solid line). We take here $\omega_{32} = 0$, $\gamma' = 0.3\Gamma_0$, $\gamma'' = 0$, $x = 1.5$, $\varphi = 0$, $\overline{\omega} = 0.632\omega_p$.

relative phase parameter. We find that the whole profile for Kerr nonlinearity is enhanced for larger distances due to the reduction of both $\Gamma_\perp$ and $\Gamma_\parallel$ reduces by distance. The nonlinear dispersion becomes zero at $\varphi = n\pi$, while it obtains its maximal amplitude for $\varphi = n\frac{\pi}{2}$. It also changes from negative to positive and back to positive as the relative phase changes from 0 to 2π.

5. Conclusion

We have studied the third-order nonlinear susceptibility behavior of a four-level closed-loop double-V-type quantum system near a plasmonic nanostructure. In the system under study, the lower V-type transition interacts with the free-space vacuum, while the upper V-type transition is affected by the interaction with localized surface plasmons. Two orthogonal circularly polarized laser fields with the same frequency and different phases and electric field amplitudes act on both transitions of the lower V-type system. A 2D array of metal-coated dielectric nanospheres is considered as a plasmonic nanostructure for which the relevant decay rates are calculated by a rigorous electromagnetic Green tensor technique.

We have shown that the presence of the plasmonic nanostructure significantly modifies the nonlinear response of the system resulting in large enhancement of the Kerr nonlinearity. In particular, the Kerr nonlinearity can be remarkably modified by increasing the distance of the quantum system from the plasmonic nanostructure. Phase control of the Kerr nonlinearity has also been discussed for such a quantum system. A wide range of tunability has been observed over the Kerr nonlinear response through the effect of the relative phase. Such a mechanism for phase control of the Kerr nonlinearity may be realized by the state-of-the-art nanomethods and it may find application in on-chip photonic nonlinear devices.

Declaration of competing interest

The authors declare that they have no known competing financial interests or personal relationships that could have appeared to influence the work reported in this paper.

Acknowledgments

This research was funded by the European Social Fund under Grant No. 09.3.3-LMT-K-712-01-0051. We acknowledge useful discussions with S.H. Asadpour.

A. Explicit expressions for $\rho_{ij}^{(2)}$

The expressions for the steady-state solutions $\rho_{ij}^{(2)}$ are:

$$\rho_{11}^{(2)} = -\frac{(r+s)}{2\gamma'}, \tag{44}$$

$$\rho_{22}^{(2)} = \frac{2\gamma'\kappa r + \kappa\gamma(r+s)}{4\gamma'\kappa(\gamma+\gamma')}, \tag{45}$$

$$\rho_{33}^{(2)} = \frac{2\gamma'\kappa s + \kappa\gamma(r+s)}{4\gamma'\kappa(\gamma+\gamma')}, \tag{46}$$

$$\rho_{23}^{(2)} = \frac{\kappa(r+s) - 2\gamma' t}{2\gamma'(i\omega_{32} - 2\gamma - 2\gamma')}, \tag{47}$$

and $\rho_{00}^{(2)} = 0$, where

$$t = \frac{i\Omega_a}{2}\Big(-i\frac{\Omega_b}{2}e^{i\varphi}S_3^* + i\kappa\frac{\Omega_a}{2}S_2^*\Big) - i\frac{\Omega_b}{2}e^{i\varphi}\Big(i\frac{\Omega_a}{2}S_1 - i\kappa\frac{\Omega_b}{2}e^{-i\varphi}S_2\Big), \tag{48}$$

$$r = \frac{i\Omega_a}{2}\Big(\Big(-i\frac{\Omega_a}{2}S_1^* + i\kappa\frac{\Omega_b}{2}e^{i\varphi}S_2^*\Big) - \Big(i\frac{\Omega_a}{2}S_1 - i\kappa\frac{\Omega_b}{2}e^{-i\varphi}S_2\Big)\Big), \tag{49}$$

$$s = \frac{i\Omega_b}{2}\Big(\Big(-i\frac{\Omega_b}{2}e^{i\varphi}S_3^* + i\kappa\frac{\Omega_a}{2}S_2^*\Big)e^{-i\varphi} - \Big(i\frac{\Omega_b}{2}e^{-i\varphi}S_3 - i\kappa\frac{\Omega_a}{2}S_2\Big)e^{i\varphi}\Big) \tag{50}$$

B. Explicit expressions for A, B, C, D, and f_i

The expressions for the coefficients A, B, C and D are:

$$A = e^{-i\varphi}x, \tag{51}$$

$$B = 1, \tag{52}$$

$$C = \frac{1}{8}\Big[-\frac{2\gamma' f_1 + \gamma f_2}{4\gamma'(\gamma+\gamma')} - \frac{\kappa f_3 + 2\gamma' f_4}{2\gamma'(-i\omega_{32} - 2\gamma - 2\gamma')}\Big], \tag{53}$$

$$D = \frac{1}{8}\Big[-\frac{2\gamma' f_5 + \gamma f_6}{4\gamma'(\gamma+\gamma')} - \frac{\kappa f_7 + 2\gamma' f_8}{2\gamma'(i\omega_{32} - 2\gamma - 2\gamma')}\Big], \tag{54}$$

with

$$f_1 = -x^3 e^{-i\varphi}(S_3 + S_3^*) + x^2\kappa e^{-2i\varphi}S_2^* + \kappa x^2 S_2, \tag{55}$$

$$f_2 = -xe^{-i\varphi}(S_1 + S_1^*) + \kappa x^2(S_2 + S_2^*) - x^3 e^{-i\varphi}(S_3 + S_3^*) - \kappa x^2 e^{-2i\varphi}(S_2 - S_2^*), \tag{56}$$

$$f_3 = -(S_1 + S_1^*) + \kappa x e^{-i\varphi}S_2 + x\kappa e^{i\varphi}S_2^* - x^2 S_3 + x\kappa S_2 e^{i\varphi} - x^2 e^{i\varphi}S_3^* + \kappa x S_2^* e^{-i\varphi}, \tag{57}$$

$$f_4 = xe^{-i\varphi}(S_3 + S_1^*) - \kappa S_2 - x^2\kappa S_2^*, \tag{58}$$

$$f_5 = (S_1 + S_1^*) - x\kappa S_2^* - \kappa x S_2 e^{-i\varphi}, \tag{59}$$

$$f_6 = (S_1 + S_1^*) - \kappa x(e^{i\varphi}S_2^* + S_2 e^{-i\varphi} + S_2^* e^{-i\varphi} + S_2 e^{i\varphi}) + x^2(S_3 + S_3^*), \tag{60}$$

$$f_7 = xe^{-i\varphi}(S_1 + S_1^*) - \kappa x^2(S_2 + S_2^*) - \kappa x^2 e^{-2i\varphi}(S_2 + S_2^*) + x^3(e^{-i\varphi}S_3 + S_3^*), \tag{61}$$

$$f_8 = -x^2 S_3^* + x\kappa e^{-i\varphi}S_2^* - x^2 S_1 + \kappa x^3 S_2 e^{-i\varphi}. \tag{62}$$

C. Explicit expressions for the resonant coefficients $\mathrm{Im}(\chi^{(1,3)}(\delta))$ and $\mathrm{Re}(\chi^{(1,3)}(\delta))$

Setting $\omega_{32} = 0$ and $\delta = 0$, Eqs. (36) and (37) and their corresponding coefficients given in Appendix B simplify, resulting in the following analytical expressions for the linear absorption/dispersion, and third-order (Kerr) nonlinear absorption/dispersion susceptibilities

$$\mathrm{Im}(\chi^{(1)}(\delta=0)) = \frac{N\mu'^2}{\epsilon_0\hbar}\frac{\gamma+\gamma'-\kappa x\cos(\varphi)}{(\gamma+\gamma')^2-\kappa^2}, \tag{63}$$

$$\mathrm{Re}(\chi^{(1)}(\delta=0)) = \frac{N\mu'^2}{\epsilon_0\hbar}\frac{-\kappa A\sin(\varphi)}{(\gamma+\gamma')^2-\kappa^2}, \tag{64}$$

$$\mathrm{Im}(\chi^{(3)}(\delta=0)) = \frac{2N\mu'^4}{3\epsilon_0\hbar^3}\frac{-m_1\cos(\varphi) - m_2\cos(2\varphi) - m_3}{32\gamma'(\gamma+\gamma')((\gamma+\gamma')^2-\kappa^2)^2}, \tag{65}$$

$$\mathrm{Re}(\chi^{(3)}(\delta=0)) = \frac{2N\mu'^4}{3\epsilon_0\hbar^3}\frac{-m_4\sin(\varphi)-m_2\sin(2\varphi)}{32\gamma'(\gamma+\gamma')((\gamma+\gamma')^2-\kappa^2)^2}, \tag{66}$$

where

$$\begin{aligned} m_1 = {} & 4\gamma' x^3\kappa(\gamma+\gamma') - 6x\kappa\gamma(\gamma+\gamma') + 2\gamma x^3\kappa(\gamma+\gamma') \\ & -4\kappa^3 x - \kappa^2 x^2(\gamma+\gamma') - 7\gamma'\kappa x(\gamma+\gamma') \\ - \quad & 4\kappa x\gamma(\gamma+\gamma') - 2x\kappa(\gamma+\gamma')^2 - \kappa x^3(\gamma+\gamma')^2 \\ & -\gamma'\kappa x^3(\gamma+\gamma'), \end{aligned} \tag{67}$$

$$m_2 = 2\kappa^2 x^2\gamma' + 2\kappa^2 x^2(\gamma+\gamma'), \tag{68}$$

$$\begin{aligned} m_3 = {} & 2\kappa^2(\gamma+\gamma')(1+2x^2) + 2\gamma'\kappa^2(1-x^2) \\ & -2\gamma'\kappa x(\gamma+\gamma') \\ & -\kappa x^3(\gamma+\gamma')^2 + 4\gamma'(\gamma+\gamma')^3(x^2-1), \end{aligned} \tag{69}$$

$$\begin{aligned} m_4 = {} & 3\kappa\gamma' x^3(\gamma+\gamma') + 2\gamma x^3\kappa(\gamma+\gamma') - \kappa^2 x^2(\gamma+\gamma') \\ & -5\gamma' x\kappa(\gamma+\gamma') - 2x\kappa(\gamma+\gamma')^2 - \kappa x^3(\gamma+\gamma'). \end{aligned} \tag{70}$$

D. EM Green's tensor for a 2D periodic nanostructure

The classical EM Green's tensor is defined through the following equation:

$$\nabla\times\nabla\times\mathbf{G}(\mathbf{r},\mathbf{r}';\omega) - k^2\mathbf{G}(\mathbf{r},\mathbf{r}';\omega) = \mathbf{1}_3\cdot\delta(\mathbf{r}-\mathbf{r}'), \tag{71}$$

where $k=\sqrt{\varepsilon_d}\omega/c$ is the wavevector inside the material, ω is the angular frequency of incident light, c is the speed of light in vacuum, and $\mathbf{1}_3$ is the 3×3 unit matrix.

We deal with arrays of macroscopic spheres with 2D periodicity. The method employed here is an EM Green's tensor formalism based on an EM layer-multiple-scattering (LMS) method [53,54]. The LMS method is ideally suited for the calculation of the transmission/reflection/absorption coefficients of an EM wave incident on slab containing a number of planes of non-overlapping scatterers with the same 2D periodicity. Namely, for each one plane of spheres, the method determines the full multipole expansion of the total multiply scattered wave field and deduces the corresponding transmission and reflection matrices of the while slab in the plane-wave basis. Having determined the transmission/reflection matrices via the LMS method one can the calculate the EM Green's tensor from [13,55]

$$\begin{aligned} & G^{EE}_{ii'}(\mathbf{r},\mathbf{r}';\omega) = g^{EE}_{ii'}(\mathbf{r},\mathbf{r}';\omega) \\ & -\frac{i}{8\pi^2}\iint_{SBZ} d^2\mathbf{k}_\parallel \sum_{\mathbf{g}}\frac{1}{c^2K^+_{\mathbf{g};z}}\times \\ & v_{\mathbf{g}\mathbf{k}_\parallel;i}(\mathbf{r})\exp(-i\mathbf{K}^+_{\mathbf{g}}\cdot\mathbf{r})\widehat{\mathbf{e}}_{i'}(\mathbf{K}^+_{\mathbf{g}}), \end{aligned} \tag{72}$$

with

$$v_{\mathbf{g}\mathbf{k}_\parallel;i}(\mathbf{r}) = \sum_{\mathbf{g}'} R_{\mathbf{g}';\mathbf{g}}(\omega,\mathbf{k}_\parallel)\exp(-i\mathbf{K}^-_{\mathbf{g}'}\cdot\mathbf{r})\widehat{\mathbf{e}}_i(\mathbf{K}^-_{\mathbf{g}'}), \tag{73}$$

and

$$\mathbf{K}^\pm_{\mathbf{g}} = (\mathbf{k}_\parallel+\mathbf{g},\ \pm[q^2-(\mathbf{k}_\parallel+\mathbf{g})^2]^{1/2}). \tag{74}$$

The vectors $\mathbf{g}$ correspond to the reciprocal-lattice vectors associated with the 2D periodic lattice of the plane of scatterers. $\mathbf{k}_\parallel$ is the reduced wavevector which lies within the surface Brillouin zone od the corresponding reciprocal lattice [53,54]. When $q^2=\omega^2/c^2<(\mathbf{k}_\parallel+\mathbf{g})^2$, $\mathbf{K}^\pm_{\mathbf{g}}$ defines an evanescent wave. The term $g^{EE}_{ii'}(\mathbf{r},\mathbf{r}';\omega)$ of Eq. (72) is the free-space Green's tensor and $\widehat{\mathbf{e}}_i(\mathbf{K}^\pm_{\mathbf{g}})$ denotes the polar unit vector normal to $\mathbf{K}^\pm_{\mathbf{g}}$. $R_{\mathbf{g}';\mathbf{g}}(\omega,\mathbf{k}_\parallel)$ is the reflection matrix which provides the sum (over $\mathbf{g}$'s) of reflected beams generated by the incidence of plane wave from the left of the plane of scatterers and is calculated via the LMS method [53,54]. We note that the above expression [Eq. (72)] is derived from the transverse part of the general classical-wave Green's tensor [55]. Also, in Eq. (72), the terms corresponding to *s*-polarized waves (those containing components with the azimuthal unit vector $\widehat{\mathbf{e}}_i(\mathbf{K}^\pm_{\mathbf{g}})$ normal to $\mathbf{K}^\pm_{\mathbf{g}}$) have very marginal contribution to the decay rates and have been, justifiably, neglected.

References

[1] S.M. Sadeghi, Gain without inversion in hybrid quantum dot-metallic nanoparticle systems, Nanotechnology 21 (2010) 455401.

[2] S.G. Kosionis, A.F. Terzis, S.M. Sadeghi, E. Paspalakis, Optical response of a quantum dot-metal nanoparticle hybrid interacting with a weak probe field, J. Phys. Condens. Matter 25 (2013) 45304.

[3] S.M. Sadeghi, Ultrafast plasmonic field oscillations and optics of molecular resonances caused by coherent exciton-plasmon coupling, Phys. Rev. A 88 (2013) 13831.

[4] D. Zhao, Y. Gu, J. Wu, J. Zhang, T. Zhang, B.D. Gerardot, Q. Gong, Quantum-dot gain without inversion: effects of dark plasmon-exciton hybridization, Phys. Rev. B 89 (2014) 245433.

[5] F. Carreño, M.A. Antón, V. Yannopapas, E. Paspalakis, Control of the absorption of a four-level quantum system near a plasmonic nanostructure, Phys. Rev. B 95 (2017) 195410.
[6] S.G. Kosionis, E. Paspalakis, Pump-probe optical response of semiconductor quantum dot-metal nanoparticle hybrids, J. Appl. Phys. 124 (2018) 223104.
[7] S. Evangelou, V. Yannopapas, E. Paspalakis, Transparency and slow light in a four-level quantum system near a plasmonic nanostructure, Phys. Rev. A 86 (2012) 53811.
[8] E. Paspalakis, S. Evangelou, V. Yannopapas, A.F. Terzis, Phase-dependent optical effects in a four-level quantum system near a plasmonic nanostructure, Phys. Rev. A 88 (2013) 53832.
[9] L. Wang, Y. Gu, H. Chen, J.-Y. Zhang, Y. Cui, B.D. Gerardot, Q.-H. Gong, Polarized linewidth-controllable double-trapping electromagnetically induced transparency spectra in a resonant plasmon nanocavity, Sci. Rep. 3 (2013) 2879.
[10] Z.-P. Wang, B.-L. Yu, Plasmonic control of refractive index without absorption in metallic photonic crystals doped with quantum dots, Plasmonics 13 (2018) 567.
[11] Y. You, Y.H. Qi, Y.P. Niu, S.Q. Gong, Control of electromagnetically induced grating by surface plasmon and tunneling in a hybrid quantum dot-metal nanoparticle system, J. Phys. Condens. Matter 31 (2019) 105801.
[12] A. Vafafard, M. Sahrai, V. Siahpoush, H.R. Hamedi, S.H. Asadpour, Optically induced diffraction gratings based on periodic modulation of linear and nonlinear effects for atom-light coupling quantum systems near plasmonic nanostructures, Sci. Rep. 10 (2020) 16684.
[13] V. Yannopapas, E. Paspalakis, N.V. Vitanov, Plasmon-induced enhancement of quantum interference near metallic nanostructures, Phys. Rev. Lett. 103 (2009) 63602.
[14] S. Evangelou, V. Yannopapas, E. Paspalakis, Simulating quantum interference in spontaneous decay near plasmonic nanostructures: population dynamics, Phys. Rev. A 83 (2011) 55805.
[15] S. Evangelou, V. Yannopapas, E. Paspalakis, Modifying free-space spontaneous emission near a plasmonic nanostructure, Phys. Rev. A 83 (2011) 23819.
[16] Y. Gu, L. Wang, P. Ren, J.-X. Zhang, T.-C. Zhang, J.-P. Xu, S.-Y. Zhu, Q.-H. Gong, Intrinsic quantum beats of atomic populations and their nanoscale realization through resonant plasmonic antenna, Plasmonics 7 (2012) 33.
[17] Y. Gu, L. Wang, P. Ren, J.-X. Zhang, T.-C. Zhang, O.J.F. Martin, Q.-H. Gong, Surface-plasmon-induced modification on the spontaneous emission spectrum via subwavelength-confined anisotropic purcell factor, Nano Lett. 12 (2012) 2488.
[18] W. Zhang, A.O. Govorov, G.W. Bryant, Semiconductor-metal nanoparticle molecules: hybrid excitons and the nonlinear fano effect, Phys. Rev. Lett. 97 (2006) 146804.
[19] R.D. Artuso, G.W. Bryant, Strongly coupled quantum dot-metal nanoparticle systems: exciton-induced transparency discontinuous response and suppression as driven quantum oscillator effects, Phys. Rev. B 82 (2010) 195419.
[20] M.R. Singh, D.G. Schindel, A. Hatef, Dipole-dipole interaction in a quantum dot and metallic nanorod hybrid system, Appl. Phys. Lett. 99 (2011) 181106.
[21] S.G. Kosionis, A.F. Terzis, V. Yannopapas, E. Paspalakis, Nonlocal effects in energy absorption of coupled quantum dot-metal nanoparticle systems, J. Phys. Chem. C 116 (2012) 23663.
[22] A.V. Malyshev, V.A. Malyshev, Optical bistability and hysteresis of a hybrid metal-semiconductor nanodimer, Phys. Rev. B 84 (2011) 35314.
[23] B.S. Nugroho, V.A. Malyshev, J. Knoester, Tailoring optical response of a hybrid comprising a quantum dimer emitter strongly coupled to a metallic nanoparticle, Phys. Rev. B 92 (2015) 165432.
[24] F. Carreño, M.A. Antón, E. Paspalakis, Nonlinear optical rectification and optical bistability in a coupled asymmetric quantum dot-metal nanoparticle hybrid, J. Appl. Phys. 124 (2018) 113107.
[25] M.R. Singh, Enhancement of the second-harmonic generation in a quantum dot-metallic nanoparticle hybrid system, Nanotechnology 24 (2013) 125701.
[26] S. Evangelou, second-order nonlinear optical effects in coupled quantum dot-metallic nanosphere structures using the purcell effect, Microelectron. Eng. 215 (2019) 111019.
[27] S. Evangelou, C.T. Angelis, Using the purcell effect for the modification of third-harmonic generation in a quantum dot near a metallic nanosphere, Optic Commun. 447 (2019) 36.
[28] J.-B. Li, N.-C. Kim, M.-T. Cheng, L. Zhou, Z.-H. Hao, Q.-Q. Wang, Optical bistability and nonlinearity of coherently coupled exciton-plasmon systems, Optic Express 20 (2012) 1856.
[29] E. Paspalakis, S. Evangelou, S.G. Kosionis, A.F. Terzis, Strongly modified four-wave mixing in a coupled semiconductor quantum dot-metal nanoparticle system, J. Appl. Phys. 115 (2014) 83106.
[30] S.K. Singh, M.K. Abak, M.E. Tasgin, Enhancement of four-wave mixing via interference of multiple plasmonic conversion paths, Phys. Rev. B 93 (2016) 35410.
[31] Y.-P. Niu, S.-Q. Gong, R.-X. Li, Z.-Z. Xu, X.-Y. Liang, Giant kerr nonlinearity induced by interacting dark resonances, Opt. Lett. 30 (2005) 3371.
[32] H. Schmidt, A. Imamog¯lu, Giant kerr nonlinearities obtained by electromagnetically induced transparency, Opt. Lett. 21 (1996) 1936.
[33] H. Wang, D. Goorskey, M. Xiao, Enhanced kerr nonlinearity via atomic coherence in a three-level atomic system, Phys. Rev. Lett. 87 (2001) 73601.
[34] Y.-P. Niu, S.-Q. Gong, Enhancing kerr nonlinearity via spontaneously generated coherence, Phys. Rev. A 73 (2006) 53811.
[35] H.R. Hamedi, G. Juzeliun¯as, Phase-sensitive kerr nonlinearity for closed-loop quantum systems, Phys. Rev. A 91 (2015) 53823.
[36] A. Imamog¯lu, H. Schmidt, G. Woods, M. Deutsch, Strongly interacting photons in a nonlinear cavity, Phys. Rev. Lett. 79 (1997) 1467.
[37] M.M. Kash, V.A. Sautenkov, A.S. Zibrov, L. Hollberg, G.R. Welch, M.D. Lukin, Y. Rostovtsev, E.S. Fry, M.O. Scully, Ultraslow group velocity and enhanced nonlinear optical effects in a coherently driven hot atomic gas, Phys. Rev. Lett. 82 (1999) 5229.
[38] X.-N. Liu, N. Kongsuwan, X.-G. Li, D.-X. Zhao, Z.-M. Wu, O. Hess, X.-H. Zhang, Tailoring the third-order nonlinear optical property of a hybrid semiconductor quantum dot-metal nanoparticle: from saturable to fano-enhanced absorption, J. Phys. Chem. Lett. 10 (2019) 7594.
[39] S. Evangelou, V. Yannopapas, E. Paspalakis, Modification of kerr nonlinearity in a four-level quantum system near a plasmonic nanostructure, J. Mod. Optic. 61 (2014) 1458.
[40] H. Chen, J. Ren, Y. Gu, D.-X. Zhao, J. Zhang, Q. Gong, Nanoscale kerr nonlinearity enhancement using spontaneously generated coherence in plasmonic nanocavity, Sci. Rep. 5 (2016) 18315.
[41] A.F. Terzis, S.G. Kosionis, J. Boviatsis, E. Paspalakis, Nonlinear optical susceptibilities of semiconductor quantum dot - metal nanoparticle hybrids, J. Mod. Optic. 63 (2016) 451.
[42] J. Ren, H. Chen, Y. Gu, D.-X. Zhao, H. Zhou, J. Zhang, Q. Gong, Plasmon-enhanced kerr nonlinearity via subwavelength-confined anisotropic purcell factors, Nanotechnology 27 (2016) 425205.
[43] M.M. Tohari, A. Lyras, M.S. AlSalhi, Giant self-kerr nonlinearity in the metal nanoparticles-graphene nanodisks-quantum dots hybrid systems under low-intensity light irradiance, Nanomaterials 8 (2018) 521.
[44] S.G. Kosionis, E. Paspalakis, Control of self-kerr nonlinearity in a driven coupled semiconductor quantum dot-metal nanoparticle structure, J. Phys. Chem. C 123 (2019) 7308.
[45] X. Liu, N. Kongsuwan, X.-G. Li, D.-X. Zhao, Z.-M. Wu, O. Hess, X.-H. Zhang, Tailoring the third-order nonlinear optical property of a hybrid semiconductor quantum dot-metal nanoparticle: from saturable to fano-enhanced absorption, J. Phys. Chem. Lett. 10 (2019) 7594–7602.
[46] G.S. Agarwal, Anisotropic vacuum-induced interference in decay channels, Phys. Rev. Lett. 84 (2000) 5500.
[47] M. Kiffner, M. Macovei, J. Evers, C.H. Keitel, Chapter 3 - vacuum-induced processes in multilevel atoms, Prog. Optic 55 (2010) 85.
[48] Y. Yang, J. Xu, H. Chen, S. Zhu, Quantum interference enhancement with left-handed materials, Phys. Rev. Lett. 100 (2008) 43601.
[49] G.-X. Li, J. Evers, C.H. Keitel, Spontaneous emission interference in negative-refractive-index waveguides, Phys. Rev. B 80 (2009) 45102.
[50] P.K. Jha, X. Ni, C. Wu, Y. Wang, X. Zhang, Metasurface-enabled remote quantum interference, Phys. Rev. Lett. 115 (2015) 25501.
[51] S. Hughes, G.S. Agarwal, Anisotropy-induced quantum interference and population trapping between orthogonal quantum dot exciton states in semiconductor cavity systems, Phys. Rev. Lett. 118 (2017) 63601.
[52] V. Karanikolas, E. Paspalakis, Plasmon-induced quantum interference near carbon nanostructures, J. Phys. Chem. C 122 (2018) 14788.
[53] N. Stefanou, V. Yannopapas, A. Modinos, Heterostructures of photonic crystals: frequency bands and transmission coefficients, Comput. Phys. Commun. 113 (1998) 49.
[54] N. Stefanou, V. Yannopapas, A. Modinos, Multem 2: a new version of the program for transmission and band-structure calculations of photonic crystals, Comput. Phys. Commun. 132 (2000) 189.
[55] R. Sainidou, N. Stefanou, A. Modinos, Green's function formalism for phononic crystals, Phys. Rev. B 69 (2004) 64301.
[56] D. Bortman-Arbiv, A.D. Wilson-Gordon, H. Friedmann, Phase control of group velocity: from subluminal to superluminal light propagation, Phys. Rev. A 63 (2001) 43818.
[57] S. Sharma, T.N. Dey, Phase-induced transparency-mediated structured-beam generation in a closed-loop tripod configuration, Phys. Rev. A 96 (2017) 33811.